Contrasting Growth Modes of Mn on Ge(100) and Ge(111) Surfaces: Subsurface Segregation versus Intermixing

Wenguang Zhu,[1,2] H. H. Weitering,[3,1] E. G. Wang,[2] Efthimios Kaxiras,[4] and Zhenyu Zhang[1,3,4]

[1]*Condensed Matter Sciences Division, Oak Ridge National Laboratory, Oak Ridge, Tennessee 37831, USA*

[2]*International Center for Quantum Structures and Institute of Physics, Chinese Academy of Sciences, Beijing 100080, People's Republic of China*

[3]*Department of Physics and Astronomy, The University of Tennessee, Knoxville, Tennessee 37996, USA*

[4]*Department of Physics and Division of Engineering and Applied Sciences, Harvard University, Cambridge, Massachusetts 02138, USA*

(Received 6 April 2004; published 16 September 2004)

Based on first-principles total energy calculations within density functional theory, we show that a low dose of Mn on Ge(100) initiates in a novel subsurface growth mode, characterized by easy access to, and strong preference for, interstitial sites located between the two topmost Ge layers. Strikingly, such a ''subsurfactant action'' is preserved even during epitaxial growth of additional Ge layers, analogous to the well-known phenomenon of surfactant action. In contrast, along the [111] orientation, Mn can easily diffuse into the bulk via interstitial sites. These results are discussed within the context of dopant control in dilute magnetic semiconductors.

DOI: 10.1103/PhysRevLett.93.126102 PACS numbers: 68.65.–k, 68.55.Ln, 75.70.–i

In today's drive for novel materials, it is often highly desirable to fabricate heterostructures with atomically abrupt interfaces and homogeneous compounds with precisely controlled stoichiometry. Such materials are typically unstable from thermodynamic equilibrium considerations but can be synthesized using nonequilibrium growth techniques such as molecular beam epitaxy (MBE). Recent studies of thin film epitaxy have led to a wealth of conceptual advances in nonequilibrium growth. One compelling example is the discovery of ''surfactant action'' in heteroepitaxy (*A*-on-*B* epitaxial growth), referring to the phenomenon that a low dose of a third element *C* serving as surface active agent (the surfactant) on the substrate *B* can drastically modify the growth mode of *A* [1,2]. As a new layer of atoms is deposited onto the surfactant-covered substrate, the surfactant atoms keep floating at the growth front while promoting layer-by-layer growth to a thickness much larger than what would be achievable without the surfactant.

Progress in the fundamental understanding of nonequilibrium growth has in turn enabled important discoveries of novel classes of materials with intriguing physical properties. Dilute magnetic semiconductors (DMS) are one such example [3,4]. In these materials, when magnetic dopants such as Mn are incorporated by MBE into a semiconductor such as GaAs at concentrations greatly exceeding the thermodynamic solubility limit, the ferromagnetic ordering temperature can be significantly enhanced [3]. More recently, ferromagnetic ordering has also been observed in Mn_xGe_{1-x}, offering a better opportunity for integrating magnetism with existing silicon technology [4]. To date, the precise microscopic mechanism for ferromagnetic ordering in DMS remains an active subject of research [5–8]. Efforts to explore various possible ordering mechanisms will undoubtedly benefit from a detailed knowledge of the magnetic dopant distribution and dopant diffusion in the semiconductors. In particular, the ordering temperature, T_C, may depend sensitively on the relative populations of interstitial and substitutional dopants, as emphasized recently for DMS based on III-V semiconductors [8–10]. In order to tune the relative populations of the dopants for higher T_C, it is imperative to know the energetic and kinetic characteristics of the newly deposited dopants at the growth front.

In this Letter, we carry out a comparative study of the energetics and kinetics involved in Mn growth on Ge along the [100] and [111] orientations, using extensive total energy calculations within density functional theory (DFT). The main findings are intriguing both from the point of view of fundamental growth science and for improved understanding of the system as a DMS. First, we show that, along the [100] orientation, the growth of Mn proceeds in a subsurface mode, characterized by their easy access to, and strong preference for, interstitial sites located between the two topmost Ge layers. Strikingly, such a ''subsurfactant action'' is preserved even during epitaxial growth of additional Ge capping layers, as shown by the existence of easy kinetic pathways for the dopants trapped in deeper layers to float toward the subsurface sites. In contrast, during growth along the [111] orientation, Mn can easily diffuse into the bulk via interstitial sites. The importance of these findings will be discussed within the context of dopant control via growth manipulation and postannealing in dilute magnetic semiconductors.

The spin-polarized DFT results reported here are based on the Perdew-Wang 1991 version of the generalized gradient approximation (PW91-GGA) [11] and were ob-

tained using VASP [12]. Default plane-wave cutoffs, 16.7 Ry, from the GGA ultrasoft-pseudopotential database [13] are used for both Mn and Ge in the calculations. The Monkhorst-Pack scheme [14] is used for Brillouin zone sampling. These choices produce a bulk lattice constant of 5.76 Å for Ge, compared to the experimental value of 5.66 Å. Optimized atomic geometries are achieved until the forces on all the unconstrained atoms are smaller than 0.03 eV/Å. The "climbing image nudged elastic band" method [15] is applied to locate the transition state geometries for calculations of the diffusion barriers.

In order to calculate adsorption and diffusion properties of a Mn adatom on the Ge(100)-2 × 1 reconstructed surface with asymmetric dimers, we use a 4 × 4 supercell containing eight layers of bulk Ge, a surface layer with the asymmetric dimer reconstruction, and a 13 Å-wide vacuum gap. The two layers at the bottom of the slab are fixed to their bulk positions, with all other layers fully relaxed. The bottom layer is passivated with H atoms. The Brillouin zone is sampled using the k point at (0.5, 0.5, 0) as in the case of Mn on Si(100) [16].

We first discuss the Mn binding energies and diffusion pathways within the surface layer. The most stable adsorption site for a Mn adatom on a Ge(100)-2 × 1 surface is the interstitial site, I_0, located 2.2 Å beneath the Ge dimer with an absolute binding energy of 3.03 eV, defined as the energy required to separate a single Mn atom from the Ge surface. The asymmetric dimer becomes almost symmetric when a Mn adatom is placed at this interstitial site. The other local metastable adsorption sites are hollow sites H and pedestal sites P, as shown in Fig. 1(a). The total energies of the system for a Mn adatom adsorbed at H and at P are 0.64 and 0.63 eV higher than that of the interstitial site, respectively. Unlike the case of the GaAs(100) surface [10], the substitutional site above the surface dimer is not even a metastable site, and a Mn adatom located above the dimer row can dive into the pedestal site with essentially no energy barrier.

Calculations of the diffusion barriers for a Mn adatom on the Ge(100)-2 × 1 surface show that the Mn adatom at the pedestal site P can slide into the subsurface interstitial site I_0 by overcoming an energy barrier of 0.59 eV, whereas the activation energy (AE) of the reverse process is 1.22 eV. These and other activation energies shown in Fig. 1(c) indicate that Mn diffuses relatively easily among the H and P sites, but once it dives *into* a subsurface interstitial site I_0 from either H or P, it will be much harder for it to hop out.

The site energies and diffusion pathways of Mn in deeper layers are shown in Figs. 1(b), 1(d), and 1(e). When a Mn atom dives deeper into the bulk, the system becomes less stable. The barriers for interstitial diffusion of Mn atoms are illustrated in Fig. 1(d). There is a very clear tendency for deeper Mn atoms to float toward the

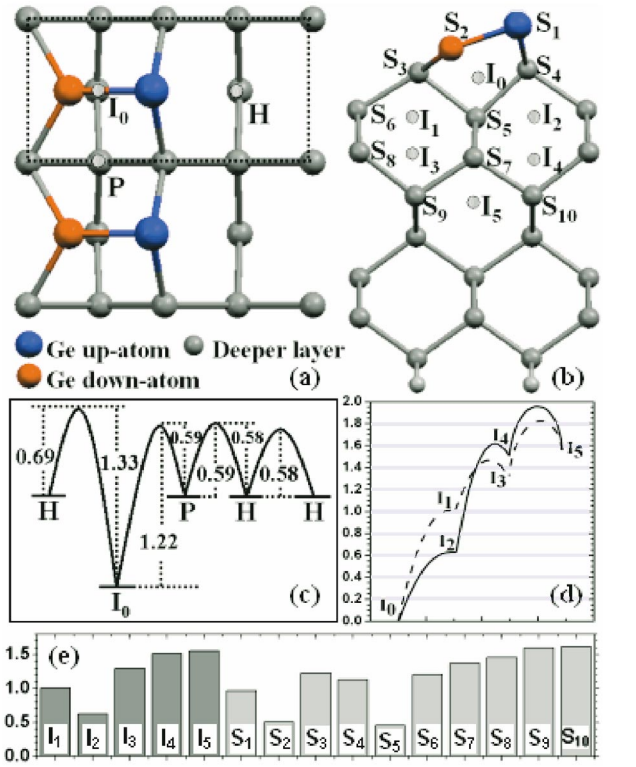

FIG. 1 (color). (a) Top view of the Ge(100)-2 × 1 surface showing the three different adsorption sites for Mn adatoms: hollow site (H), pedestal site (P) and interstitial site (I_0). (b) Side view of the Ge(100)-2 × 1 surface geometry showing the various interstitial and substitutional sites. (c) Diffusion barriers for a Mn adatom on Ge(100)-2 × 1. (d) Diffusion barriers between interstitial sites beneath the Ge(100)-2 × 1 surface. (e) Total energies of interstitial and substitutional sites relative to that of I_0. All the energies are in eV.

subsurface interstitial site I_0: For example, the pathway $I_5 \rightarrow I_3 \rightarrow I_1 \rightarrow I_0$ involves a highest AE of only 0.27 eV, while the pathway $I_5 \rightarrow I_4 \rightarrow I_2 \rightarrow I_0$ involves a highest AE of only 0.37 eV. The other potentially stable sites for a Mn atom are the substitutional sites where the Mn atom substitutes a Ge atom. We estimate the relative stability of Mn in interstitial sites and substitutional sites by introducing μ_{Ge}, the chemical potential of Ge, which corresponds to the total energy of a Ge atom in bulk Ge. All of the substitutional sites shown in Fig. 1(b) are less stable than the interstitial site I_0. The total energies relative to I_0 are shown in Fig. 1(e). In contrast, the Mn atom prefers to be substitutional in bulk Ge by as much as 0.41 eV, according to our bulk calculations.

In order to substitute a Ge atom, the Mn atom must displace a Ge atom to a neighboring interstitial site. To estimate the energy cost of this process, we put the Mn atom at the S_5 site, as an example, which is the most stable substitutional site in our calculations. The S_5 Ge atom is displaced toward the neighboring interstitial sites

I_0, I_1, I_2, I_3, and I_4, respectively. The total energies of these configurations are at least 1.1 eV higher than that of the configuration where the Mn atom resides at I_0. The AE of this process should be even higher.

The results can be summarized as follows. In a (100) surface environment, Mn strongly prefers the I_0 interstitial site. Furthermore, the diffusion kinetics indicates that Mn should diffuse toward I_0, regardless of whether Mn originates from the gas phase above the surface or from the bulk. Even though the substitutional site is favored inside the bulk, the kinetic barrier for substitutional incorporation is too high. Therefore, low-temperature MBE of Mn-doped Ge(100) DMS should result in a high density of interstitial Mn. As Mn atoms are buried beneath a newly deposited Ge layer, they tend to float upward toward the I_0 sites.

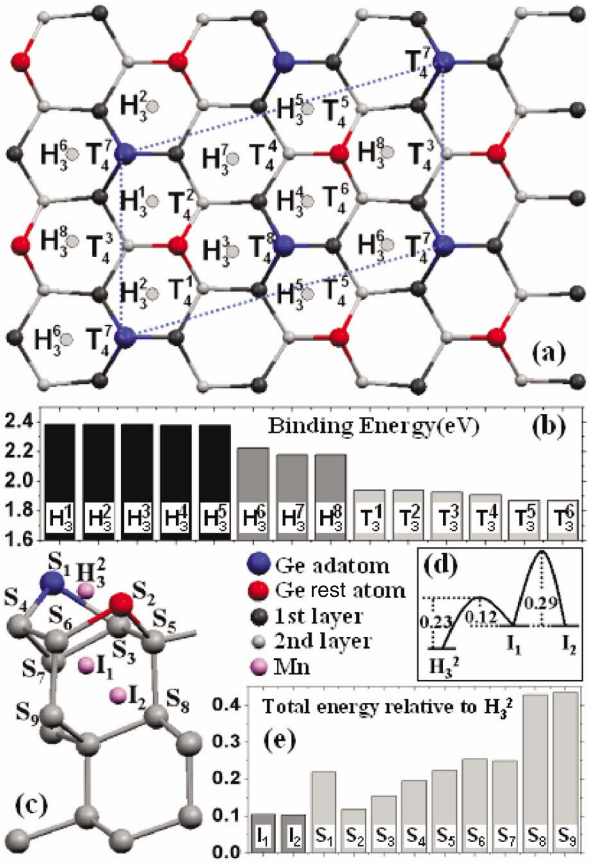

FIG. 2 (color). (a) Top view of the Ge(111)-$c(2 \times 8)$ surface indicating the various adsorption sites for a Mn adatom. (b) Binding energy of a Mn adatom at different sites on the Ge(111)-$c(2 \times 8)$. (c) Side view of the Ge(111)-$c(2 \times 8)$ surface showing the various interstitial and substitutional sites. (d) Energy barriers for Mn diffusion between the interstitial sites on Ge(111)-$c(2 \times 8)$. (e) Total energies of the interstitial and substitutional sites relative to that of the $H_3{}^2$ site. All the energies are in eV.

Now we turn to Mn growth on Ge(111). The surface of Ge(111) at room temperature exhibits a $c(2 \times 8)$ reconstruction, in which each Ge adatom saturates three surface dangling bonds, while one-quarter of the surface dangling bonds remains uncovered. The equilibrium $c(2 \times 8)$ periodicity is made up of (2×2) and $c(2 \times 4)$ subunits, each of which contains one Ge adatom and one Ge rest atom. Ge adatoms reside at the T_4 site, which is located directly above an atom belonging to the lower half of the surface bilayer. In calculating the adsorption energies and diffusion barriers on the $c(2 \times 8)$ surface, we use a large supercell, corresponding to two primitive $c(2 \times 8)$ unit cells, and consisting of six layers with 16 Ge atoms each. Four Ge adatoms are placed at the T_4 sites of the top surface. Sixteen hydrogen atoms passivate the bottom layer of the slab. Consecutive slabs are separated by an empty space of 13 Å wide. Atoms of the bottom two Ge layers are fixed at the corresponding bulk positions, while the other atoms are fully relaxed. The k-point sampling of the surface Brillouin zone is on a 3×3 mesh.

The adsorption sites and binding energies of a Mn adatom on the Ge(111)-$c(2 \times 8)$ surface relative to the configuration where the Mn is isolated far away from the surface are illustrated in Figs. 2(a) and 2(b). The H_3 sites are energetically more favorable than the T_4 sites, a prediction confirmed experimentally [17]. Among the eight H_3 sites within a primitive $c(2 \times 8)$ cell, each of the five ($H_3{}^1$, $H_3{}^2$, $H_3{}^3$, $H_3{}^4$, $H_3{}^5$) has one neighboring Ge adatom and one neighboring Ge rest atom. These are the most favorable adsorption sites. Their energy differences are within 0.03 eV. The binding energy of a Mn adatom at any of the remaining H_3 sites ($H_3{}^6$, $H_3{}^7$, or $H_3{}^8$) is lower by approximately 0.16 eV. The T_4 sites have approximately 0.5 eV lower binding energy compared to the most stable H_3 sites. The activation energies for Mn hopping from H_3 to T_4 sites ranges from 0.5 to 0.6 eV, while the AE for the reverse processes range from 0.1 to 0.3 eV.

We have also calculated the energies of the interstitial and substitutional sites in deeper layers along the [111] orientation, as shown in Fig. 2(c). The total energies relative to the most stable adsorption site $H_3{}^2$ are shown in Fig. 2(e). In contrast to the case along the [100)] orientation, the binding energies of the interstitial sites in deeper layers are lower than that of the $H_3{}^2$ surface site, but by only 0.11 eV. Additionally, the diffusion barrier for a Mn adatom from the $H_3{}^2$ site to the I_1 site is 0.23 eV, and the AE for the reverse process is 0.12 eV. The AE for diffusion between I_1 and I_2 is 0.29 eV, as shown in Fig. 2(d).

The physical origin for the contrasting behavior of Mn along the two different orientations is tied to the relative openness of the two surfaces and to the corresponding strain built near the surface regions due to different surface reconstructions. In particular, our calculations show that when the dimerization of the Ge atoms on the

(100) surface is lifted by saturating the Ge dangling bonds with hydrogen, the stable I_0 sites become energetically unstable relative to interstitial sites that are located in deeper layers. Our results are supported by some existing experiments [18(a),18(b)], in particular, by an x-ray photoelectron spectroscopy (XPS) study of MBE growth of Mn_xGe_{1-x}, obtained by co-deposition of Mn and Ge on Ge(100)-2×1 in ultrahigh vacuum [18(c)]. A dramatic increase of the magnetic ordering temperature, upon annealing, is accompanied by a significant increase in Mn concentration near the surface layers, an observation consistent with our theory.

The theoretical results obtained here have important implications for experimental studies of Mn_xGe_{1-x} as a DMS for spintronic applications. (i) The high preference of Mn to the subsurface sites along the [100] orientation as predicted here should offer a natural pathway for formation of a high-density layer of Mn embedded into Ge, whose magnetic properties remain to be explored. (ii) For a Mn_xGe_{1-x} DMS system obtained by co-deposition of Ge and Mn, a high concentration of Mn will be trapped at interstitial sites in the bulk. If the system is initially grown along the [100] orientation, proper *in situ* annealing after growth should drive a significant percentage of the interstitial Mn atoms in the bulk toward the subsurface interstitial sites, thereby altering the relative populations of the Mn in substitutional and interstitial sites in the bulk. Such a population change may cause an increase of the magnetic ordering temperature, as in III-V DMS materials [19,20] and, most recently, also in Mn_xGe_{1-x} DMS [18(c)]. (iii) The orientation dependence of the Mn distribution under otherwise identical growth conditions should be readily observable. (iv) Similar subsurfactant action may be expected in other related systems [19–21].

In summary, we have used spin-polarized DFT calculations to map out all the important lattice locations and diffusion barriers for Mn atoms at the growth fronts along two different orientations of Ge. A novel subsurface growth phenomenon termed as subsurfactant action has been predicted in MBE growth on the Ge(100)-2×1 surface. Mn adatoms originating from the gas phase or from deeper layers in the substrate can easily diffuse toward the interstitial sites right beneath the dimers of the Ge(100)-2×1 surface reconstruction where they become trapped (the I_0 sites). As Mn atoms are buried beneath a newly deposited Ge layer, they tend to float upward toward the new I_0 sites. In contrast, no subsurfactant phenomenon has been identified for Mn growth on Ge(111), where the Mn atoms can diffuse into deeper layers with relatively low energy barriers. Several important implications of these predictions have been proposed, awaiting confirmation in future experimental studies of Mn_xGe_{1-x} as a DMS.

We thank Dr. J. X. Zhong for some initial contribution to this work and Dr. C. G. Zeng and Dr. S. C. Erwin for helpful discussions. This work was sponsored in part by the U.S. NSF (Grants No. DMR-0306239 and No. DMR-0325218), by the U.S. DOE (Grant No. DE-FG03-02ER45958), by the NSF, MOST, and CAS of China, and by the LDRD Program of Oak Ridge National Laboratory, managed by UT-Battelle, LLC, for the U.S. Department of Energy under Contract No. DE-AC05-00OR22725. The calculations were performed at DOE's NERSC and ORNL's Center for Computational Sciences.

[1] M. Copel, M. C. Reuter, E. Kaxiras, and R. M. Tromp, Phys. Rev. Lett. **63**, 632 (1989).
[2] W. F. Egelhoff and D. A. Steigerwald, J. Vac. Sci. Technol. A **7**, 2167 (1989).
[3] H. Ohno *et al.*, Appl. Phys. Lett. **69**, 363 (1996).
[4] Y. D. Park *et al.*, Science **295**, 651 (2002).
[5] T. Dietl *et al.*, Science **287**, 1019 (2000).
[6] S. Das Sarma, E. H. Hwang, and A. Kaminski, Solid State Commun. **127**, 99 (2003).
[7] T. Jungwrith *et al.*, Appl. Phys. Lett. **83**, 320 (2003).
[8] C. Timm, J. Phys. Condens. Matter **15**, R1865 (2003).
[9] K. M. Yu *et al.*, Phys. Rev. B **65**, 201303(R) (2002).
[10] S. C. Erwin and A. G. Petukhov, Phys. Rev. Lett. **89**, 227201 (2002).
[11] J. P. Perdew and Y. Wang, Phys. Rev. B **45**, 13 244 (1992).
[12] G. Kresse and J. Furthmüller, Phys. Rev. B **54**, 11 169 (1996).
[13] D. Vanderbilt, Phys. Rev. B **41**, 7892 (1990); G. Kresse and J. Hafner, J. Phys. Condens. Matter **6**, 8245 (1994).
[14] H. J. Monkhorst and J. D. Pack, Phys. Rev. B **13**, 5188 (1976).
[15] H. Jónsson, G. Mills, and K.W. Jacobsen, in *Classical and Quantum Dynamics in Condensed Phase Simulations*, edited by B. J. Berne *et al.* (World Scientific, Singapore, 1998); G. Henkelman, B. P. Uberuaga, and H. Jónsson, J. Chem. Phys. **113**, 9901 (2000).
[16] G. M. Dalpian, A. J. R. da Silva, and A. Fazzio, Phys. Rev. B **68**, 113310 (2003).
[17] C. G. Zeng, W. G. Zhu, S. C. Erwin, Z. Y. Zhang, and H. H. Weitering (to be published).
[18] (a) F. D'Orazio *et al.*, IEEE Trans. Magn. **38**, 2856 (2002); (b) L. F. Liu *et al.*, J. Cryst. Growth **265**, 466 (2004); (c) A. P. Li, C. G. Zeng, J. Shen, and H. H. Weitering (to be published).
[19] S. J. Potashnik *et al.*, Appl. Phys. Lett. **79**, 1495 (2001).
[20] K.W. Edmonds *et al.*, Phys. Rev. Lett. **92**, 037201 (2004).
[21] R. L. Headrick, I. K. Robinson, E. Vliek, and L. C. Feldman, Phys. Rev. Lett. **63**, 1253 (1989); P. Bedrossian *et al.*, *ibid.* **63**, 1257 (1989); I.W. Lyo, E. Kaxiras, and P. Avouris, *ibid.* **63**, 1261 (1989).